Journal of Sound and Vibration (2001) **241**(4), 587–604
doi:10.1006/jsvi.2000.3314, available online at http://www.idealibrary.com on IDEAL®

FINITE ELEMENT MODELLING OF INFINITE EULER BEAMS ON KELVIN FOUNDATIONS EXPOSED TO MOVING LOADS IN CONVECTED CO-ORDINATES

L. Andersen, S. R. K. Nielsen and P. H. Kirkegaard

Department of Structural Engineering, Aalborg University, Sohngaardsholmsvej 57, *DK*-9000 *Aalborg, Denmark. E-mail: la@civil.auc.dk*

(*Received* 5 *January* 2000, *and in final form* 19 *July* 2000)

The paper deals with the finite element method (FEM) solution of the problem with loads moving uniformly along an infinite Euler beam supported by a linear elastic Kelvin foundation with linear viscous damping. Initially, the problem is formulated in a moving co-ordinate system following the load using a Galilean co-ordinate transformation and subsequently the analytical solution to the homogeneous beam problem is shown. To be used in more complicated cases where no analytical solutions can be found, a numerical approach of the same problem is then suggested based on the FEM. Absorbing boundary conditions to be applied at the ends of the modelled part of the infinite beam are derived. The quality of the numerical results for single-frequency, harmonic excitation is tested by comparison with the indicated analytical solution. Finally, the robustness of the boundary condition is tested for a Ricker pulse excitation in the time domain.

1. INTRODUCTION

Wave propagation in beam-like structures resting on some type of support or medium has recently been studied extensively, especially within the fields of vehicle dynamics and railway tracks. Examples include the work done by Sheng *et al.* [1] and by Dieterman and Metrikine [2–4]. Most of the work that has been done recently concerns analytical solutions to moving load problems (see, e.g., reference [5]) finding critical velocities of wave sources [4], as well as analyzing the behaviour of waves. Hardy [6] suggested a method to determine whether travelling waves will occur when media or structures are submitted to moving harmonic loading. As an example, Hardy analyzed an Euler beam on an undamped Kelvin foundation, finding that either two or four travelling waves may occur, half of which propagate in front of the point source and the other half propagates behind the source.

To analyze complex structures, the finite element method (FEM) is useful, though in wave propagation problems one has to consider both time and spatial increments in the numerical algorithm. Specifically, Rieker *et al.* [7] found that 2–8 times more elements have to be used in analysis of moving loads on a beam than are necessary for analysis of stationary loads when a fixed system of reference is considered. Furthermore, in unbounded media one has to apply artificial boundary conditions to prevent accumulation of energy within the modelled part of the medium. Several methods have been introduced in the work by Wolf and co-workers [8–10]. An FE solution to the convention problem due to a moving load on an elastic half-space has been given by Krenk *et al.* [11] using a moving frame of reference. An analogous moving reference system was used by Metrikine and

0022-460X/01/140587 + 18 $35.00/0

Dieterman [12] in the analytical solution of the instability problem due to a point mass moving on an Euler beam–Kelvin foundation system. Concerning the FE analysis of wave propagation in beams, the work that has previously been done is, however, confined to analysis in a fixed reference system. This includes the work by Suiker *et al.* [13], who gave an FE solution to the wave yield generated by an accelerating load on a Timoshenko beam–half-space system.

In this paper, the particular convection problem of a moving load on an infinite Euler beam resting on a Kelvin foundation has been treated in a new way. Using a Galilean co-ordinate transformation, the equation of motion is formulated in a convected co-ordinate system following the point load. Furthermore, damping in the support is taken into consideration. An FEM approach to the problem, including the derivation of transparent boundary conditions, is suggested to handle complicated problems such as rail–vehicle interaction for multiple degrees-of-freedom vehicles as well as local non-linear behaviour of the beam in the vicinity of the moving force. The transmitting boundary conditions provide the interaction forces from the surrounding linear domain. Hence, the boundary conditions provide the interaction forces from the surrounding linear domain. Hence, the boundary conditions are independent of any possible non-linearities in the FE part of the structure.

The boundary conditions are derived for a single-frequency harmonic point load moving at constant velocity, but the performance will also be tested for an excitation signal containing a broad band of frequencies.

2. EQUATION OF MOTION IN CONVECTED CO-ORDINATES

A plane Euler beam with constant bending stiffness EI and mass per unit length μ is considered. Axial deformation is assumed not to take place. The beam is supported by a Kelvin foundation with constant spring stiffness κ and viscous damping γ per unit length.

Now the beam is split into two regions. One region comprises the part of the beam to be modelled with finite elements, whereas the contributions from the surroundings, i.e., the other region, to the reaction forces at the interface are incorporated by means of absorbing boundary conditions. Hence, the frequency response matrix relating the in-plane bending moment $M_b(t)$ and shear force $Q_b(t)$ to the vertical end displacement $u_b(t)$ and co-directional end rotation $\theta_b(t)$ is sought at the artificial boundary $X = X_b$, where X is a fixed co-ordinate measured along the beam axis (see Figure 1).

The beam is assumed to be free of loading except for a point force located at $X = X_P$. In a fixed co-ordinate system, the equation of motion for the rest of the beam becomes

$$EI\frac{\partial^4 u}{\partial X^4} + \kappa u + \gamma \dot{u} + \mu \ddot{u} = 0. \tag{1}$$

$u(X, t)$ is the displacement field, whereas $\dot{u}$ and $\ddot{u}$ denote the velocity and acceleration, which in fixed co-ordinates are defined, respectively, as

$$\dot{u}(X, t) = \frac{\partial u}{\partial t}, \qquad \ddot{u}(X, t) = \frac{\partial^2 u}{\partial t^2}. \tag{2}$$

A discretization of equation (1) and implementation of matching absorbing boundary conditions may prove useful for FEM analysis of stationary load problems. However, in the general case, where moving loads occur, the problem is better suited for analysis in

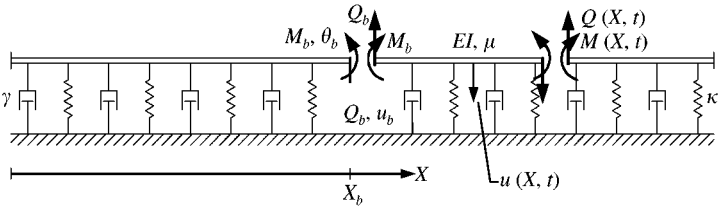

Figure 1. Plane Euler beam on Kelvin foundation.

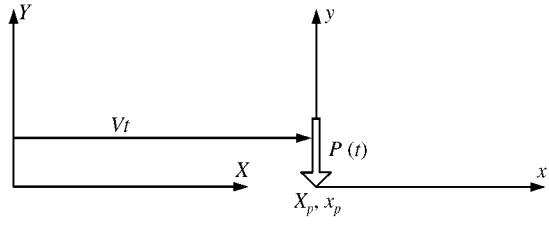

Figure 2. Fixed and moving co-ordinates, X and x.

a convected co-ordinate system. Specifically, when the load moves at the constant velocity V along the beam axis in the positive X direction, a description in convected co-ordinates is obtained by application of the *Galilean transformation*

$$x = X - Vt, \tag{3}$$

relating the fixed Cartesian co-ordinate X to the co-directional, convected co-ordinate x. As seen from equation (3) and illustrated in Figure 2, x is moving along with the point source, and the two co-ordinate systems coincide at $t = 0$.

Partial derivatives in the two co-ordinate systems are related in the following manner:

$$\frac{\partial}{\partial X} = \frac{\partial}{\partial x}, \qquad \left.\frac{\partial}{\partial t}\right|_X = \left.\frac{\partial}{\partial t}\right|_x - V\frac{\partial}{\partial x},$$
$$\left.\frac{\partial^2}{\partial t^2}\right|_X = \left.\frac{\partial^2}{\partial t^2}\right|_x - 2V\left.\frac{\partial^2}{\partial x \partial t}\right|_x + V^2\frac{\partial^2}{\partial x^2}. \tag{4}$$

Hence, in the convected co-ordinate description, the equation of motion for an Euler beam supported by a Kelvin foundation is found to be

$$EI\frac{\partial^4 u}{\partial x^4} + \kappa u + \gamma\left(\dot{u} - V\frac{\partial u}{\partial x}\right) + \mu\left(\ddot{u} - 2V\frac{\partial \dot{u}}{\partial x} + V^2\frac{\partial^2 u}{\partial x^2}\right) = 0. \tag{5}$$

Here use has been made of the fact that the displacement field is identical in fixed and moving co-ordinates, i.e., $u(x, t) = u(X, t)$, as long as x and X describe the same material point, which will be the case when equation (3) is applied.

3. DISPLACEMENT FIELD FOR HARMONIC EXCITATION

The load is assumed to vary harmonically with time at the circular frequency ω, thereby giving rise to harmonic bending waves in the beam that may or may not propagate as

travelling waves into the farfield. Furthermore, for the sake of convenience, the load is assumed to be located at $x_P = 0$ lying within the FEM modelled part of the beam. Hence, solutions to equation (5) are sought in the form

$$u(x, t) = u_0 e^{i(kx - \omega t)}, \tag{6}$$

where $i = \sqrt{-1}$ is the imaginary unit and k is the wavenumber, which is generally complex.

Insertion of the displacement field (6) into equation (5) and subsequent rearrangement of the terms lead to the characteristic polynomial

$$k^4 - \frac{\mu V^2}{EI} k^2 - \frac{(i\gamma V + 2\mu\omega V)}{EI} k + \frac{(\kappa - \mu\omega^2 - i\gamma\omega)}{EI} = 0. \tag{7}$$

Hence, there are four independent harmonic solutions to equation (5), namely the displacement fields of type (6) with wavenumbers corresponding to the four roots k_j, $j = 1, 2, 3, 4$, of equation (7). The general solution to the homogeneous differential equation (5) is a superposition of all four terms.

Alternatively, the jth wavenumber may be written as

$$k_j = \alpha_j + i\beta_j, \tag{8}$$

where α_j and β_j are the real and imaginary parts of k_j respectively. α_j represents propagation and β_j represents attenuation of the jth wave component. Furthermore, for convenience, the non-dimensional frequency, Ω, the non-dimensional convection velocity, v, as well as the damping ratio, ζ are introduced:

$$\Omega = \frac{\omega}{\omega_0}, \qquad \omega_0 = \sqrt{\frac{\kappa}{\mu}}, \qquad v = \frac{V}{V_0}, \qquad V_0 = \sqrt[4]{\frac{EI\kappa}{\mu^2}}, \tag{9, 10}$$

$$\zeta = \frac{\gamma}{\gamma_0}, \qquad \gamma_0 = 2\sqrt{\mu\kappa}. \tag{11}$$

ω_0 signifies the circular eigenfrequency of the infinite beam with respect to the vertical stiff-body mode, and v may be interpreted as some kind of Mach number since it is of order 1 when V is close to the lowest of the phase velocities $c_j = \omega/\alpha_j$.

When no convection is present it turns out that one of the wavenumbers always has positive imaginary part, except when $\Omega = 0$, $\zeta = 0$. This wavenumber will be referred to as k_1. Another wavenumber, k_2, has either a positive imaginary part or is positive and real. A third wavenumber always has a negative imaginary part, except when $\Omega = 0$, $\zeta = 0$. This wavenumber will be addressed k_3. Finally, k_4 has either a negative imaginary part or is negative and real.

Physically, only solutions with finite displacement amplitudes in the far field are acceptable and, furthermore, waves without attenuation must propagate away from the source. Henceforth, the displacement fields on each side of the source reduce to

$$u(x, t) = \begin{cases} A_1 e^{-\beta_1 x + i(\alpha_1 x - \omega t)} + A_2 e^{-\beta_2 x + i(\alpha_2 x - \omega t)}, & x > 0, \\ A_3 e^{-\beta_3 x + i(\alpha_3 x - \omega t)} + A_4 e^{-\beta_4 x + i(\alpha_4 x - \omega t)}, & x < 0, \end{cases} \tag{12}$$

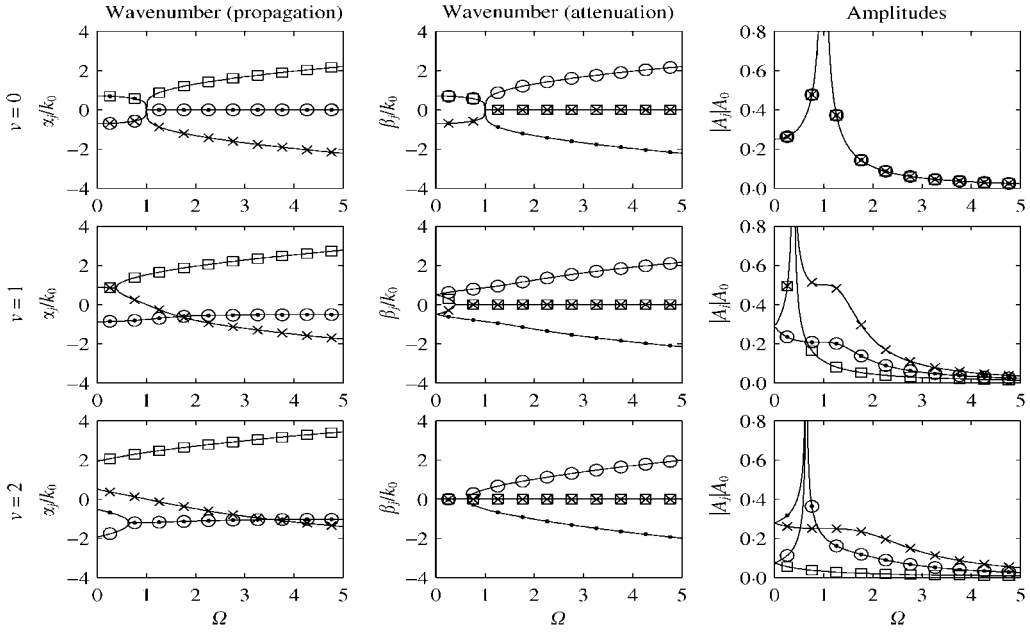

Figure 3. Nondimensional wavenumbers and amplitudes for $\zeta = 0$. Curves corresponding to the 1st, 2nd, 3rd and 4th wave component have been indicated by ○, □, • and × respectively.

where, to summarize, the following characteristics apply for $v = 0$:

$$\beta_1 > 0, \quad \beta_2 > 0 \vee \beta_2 = 0, \quad \alpha_2 > 0,$$
$$\beta_3 < 0, \quad \beta_4 < 0 \vee \beta_4 = 0, \quad \alpha_4 < 0. \tag{13}$$

When convection is introduced the wavenumbers, especially k_4, behave in a slightly different manner. Thus, for sufficiently low excitation frequency and high convection velocity the 4th wave component starts moving in the opposite direction. This, together with other phenomena, is illustrated in Figures 3–5, which show the wavenumbers' dependence on the loading frequency and the convection velocity at different levels of damping in the support. The wavenumbers and amplitudes have been normalised with respect to the parameters $k_0 = W_0/V_0$ and $A_0 = EI^{-1}k_0^{-3}$.

In the general case, where damping is present in the support, no wave propagation takes place into the far field in the form of travelling waves without attenuation, since all $\beta_j \neq 0$, see equation (12). However, when no damping is applied, it may be noticed that travelling waves without attenuation still occur only under certain circumstances, namely when $\Omega > 1$ (Figure 3), since some of the β_js here become zero. Such so-called *cut-off frequencies* as ω_0 have also been proved to exist in soil layers overlaying a bedrock [9].

It must be emphasized that a small value of α_j corresponds to a high value of c_j, especially when $\alpha_j = 0$, $|c_j| = \infty$. The wavelength is given as $\lambda_j = |c_j T_j|$ with T_j denoting the wave period which will be equal to the excitation period, T. Thus, the jth wavelength is (nearly) infinite when α_j is (close to) zero. Moreover, these waves with (nearly) infinite wavelengths are associated with a high degree of attenuation. Hence, these waves are (almost) standing waves present only within a small region near the source. There is one exception to this, namely the 4th wave component (× signature) for $v = 1$ and 2 (see Figures 4 and 5).

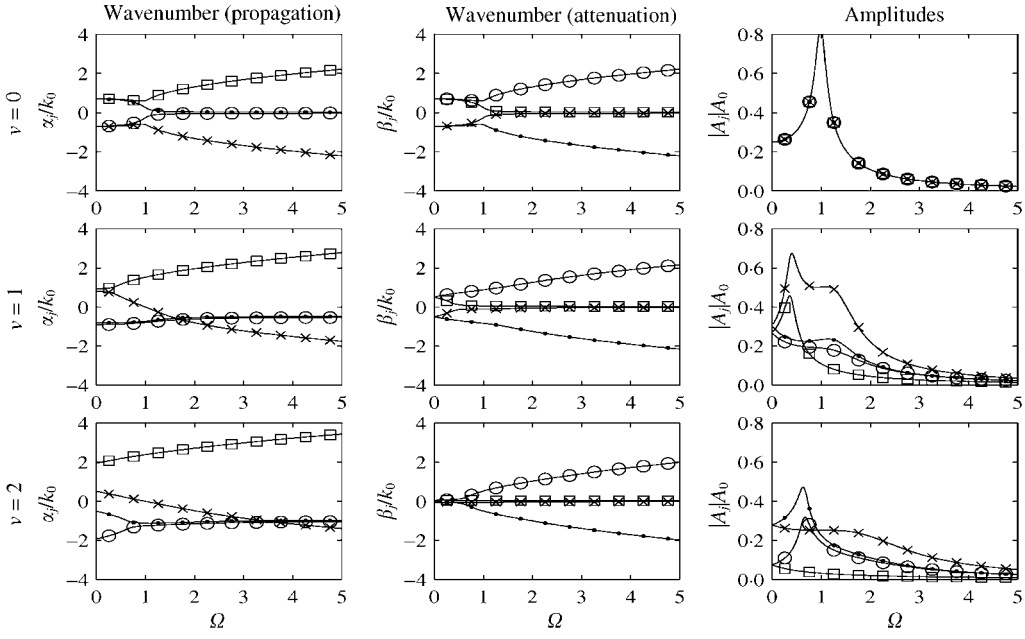

Figure 4. Nondimensional wavenumbers and amplitudes for $\zeta = 0{\cdot}1$. Curves corresponding to the 1st, 2nd, 3rd and 4th wave component have been indicated by ○, □, • and × respectively.

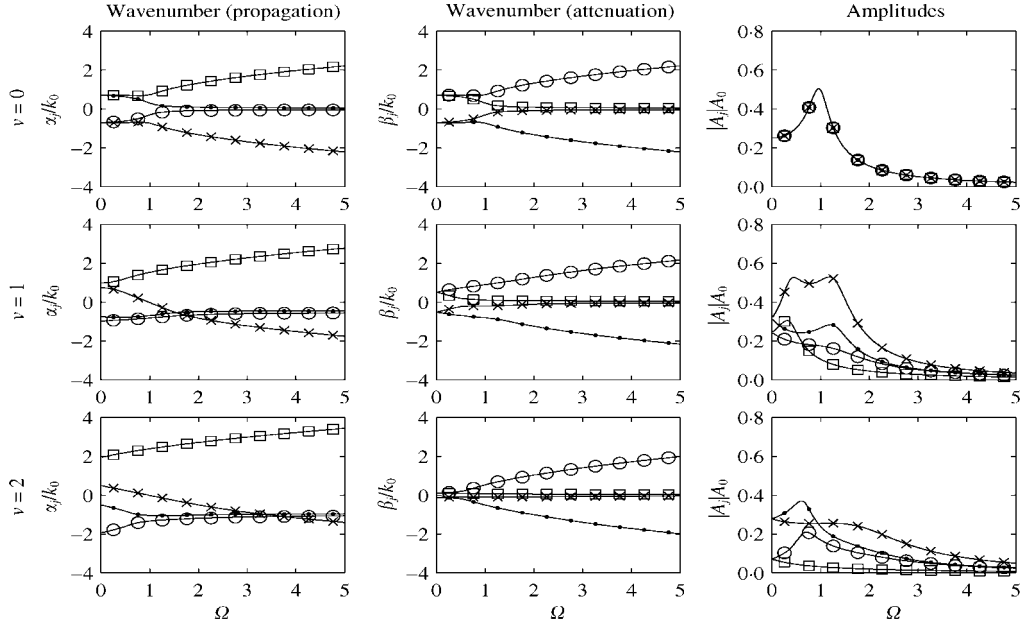

Figure 5. Nondimensional wavenumbers and amplitudes for $\zeta = 0{\cdot}2$. Curves corresponding to the 1st, 2nd, 3rd and 4th wave component have been indicated by ○, □, • and × respectively.

Here, $\alpha = 0$ for $\Omega \approx 1$, but at the same time β is very small. This observation will be returned to later.

Henceforth, note that when no convection is introduced the 1st and 3rd wave component (○ and • of Figures 3 to 5) will propagate as standing waves when $\zeta = 0$, i.e., waves with

$\alpha = 0$. These waves will, however, transform into travelling waves when $v > 0$. Furthermore, the waves that in all cases propagate as travelling waves, i.e., the 2nd and 4th wave component (□ and × of Figures 3 to 5), will propagate at a relatively higher speed behind the source and lower speed in front of the source as the level of convection increases, since the phase velocity c_j of wave propagation is proportional to α_j^{-1}. An analysis showing how many travelling waves arise for different combinations of Ω and v has previously been presented by Hardy [6] for the problem in question, although for a fixed co-ordinate system.

To complete the analytical solution, the amplitude parameters A_j must first be fitted to fulfill the following requirements at the loading point, i.e., $x_P = 0$,

$$u^-(0,t) = u^+(0,t), \qquad EI\left.\frac{\partial^2 u^-}{\partial x^2}\right|_{x=0} = EI\left.\frac{\partial^2 u^+}{\partial x^2}\right|_{x=0},$$

$$\left.\frac{\partial u^-}{\partial x}\right|_{x=0} = \left.\frac{\partial u^+}{\partial x}\right|_{x=0}, \qquad EI\left.\frac{\partial^3 u^-}{\partial x^3}\right|_{x=0} = EI\left.\frac{\partial^3 u^+}{\partial x^3}\right|_{x=0} - P_0, \tag{14}$$

where u^- and u^+ are the displacement fields at negative and positive abscissas, respectively, and P_0 is the amplitude of the harmonic excitation, i.e., $P(t) = P_0 e^{-i\omega t}$. Equation (14) provides the following four linear equations for the determination of the unknown amplitudes A_j in equation (12):

$$\begin{bmatrix} 1 & 1 & -1 & -1 \\ \eta_1 & \eta_2 & -\eta_3 & -\eta_4 \\ \eta_1^2 & \eta_2^2 & -\eta_3^2 & -\eta_4^2 \\ \eta_1^3 & \eta_2^3 & -\eta_3^3 & -\eta_4^3 \end{bmatrix} \begin{bmatrix} A_1 \\ A_2 \\ A_3 \\ A_4 \end{bmatrix} = \frac{1}{EI} \begin{bmatrix} 0 \\ 0 \\ 0 \\ P_0 \end{bmatrix}, \tag{15}$$

where $\eta_j = -\beta_j + i\alpha_j$. The amplitudes have been plotted for various combinations of damping, convection and excitation frequency in Figures 3–5 along with the corresponding wavenumbers. It is seen that there is a clear connection between peaks of the amplitudes and bifurcations on the frequency–wavenumber curves. Of special interest are the peaks at $\Omega = 1$ for $\zeta = v = 0$, which go towards ∞. On the other hand, when damping is introduced, either in the form of material damping, $\zeta > 0$, or because of the local energy loss due to convection, $v > 0$, the amplitude peaks have finite extrema. However, the (Ω, v) combinations corresponding to the peaks might still prove critical in constructional design.

4. FE TRANSMITTING BOUNDARY CONDITIONS

Subsequently, only a finite part of the beam, i.e., in the $[x_b^-, x_b^+]$-interval will be considered. Transmitting boundary conditions are to be derived for the interfaces x_b^- and x_b^+ which will constitute the end points of the FEM model. With the direction

definitions given in Figure 1 the bending moment and shear force become

$$M(x,t) = -EI\frac{\partial^2 u}{\partial x^2}, \qquad Q(x,t) = -EI\frac{\partial^3 u}{\partial x^3} \tag{16}$$

and the rotation is defined as

$$\theta(x,t) = -\frac{\partial \mathrm{u}}{\partial x}. \tag{17}$$

With these definitions and the displacement fields given by equation (12), the following relationships between amplitudes in the frequency domain for a boundary located at positive abscissas are then given:

$$\begin{bmatrix} \hat{\theta}_b^+(\omega) \\ \hat{u}_b^+(\omega) \end{bmatrix} = \mathbf{L}_0^+ \begin{bmatrix} A_1 \\ A_2 \end{bmatrix}, \qquad \mathbf{L}_0^+ = \begin{bmatrix} \beta_1 - \mathrm{i}\alpha_1 & \beta_2 - \mathrm{i}\alpha_2 \\ 1 & 1 \end{bmatrix}, \tag{18}$$

$$\begin{bmatrix} \hat{M}_b^+(\omega) \\ \hat{Q}_b^+(\omega) \end{bmatrix} = \mathbf{L}_1^+ \begin{bmatrix} A_1 \\ A_2 \end{bmatrix}, \qquad \mathbf{L}_1^+ = -EI\begin{bmatrix} (\beta_1 - \mathrm{i}\alpha_1)^2 & (\beta_2 - \mathrm{i}\alpha_2)^2 \\ (\beta_1 - \mathrm{i}\alpha_1)^3 & (\beta_2 - \mathrm{i}\alpha_2)^3 \end{bmatrix}, \tag{19}$$

where the upper index $+$ has been introduced to indicate that the parameters belong to the interface at positive abscissas and the amplitude functions $\hat{u}_b^+(\omega)$, $\hat{\theta}_b^+(\omega)$, $\hat{Q}_b^+(\omega)$ and $\hat{M}_b^+(\omega)$ are defined by

$$\begin{aligned} u_b^+(t) &= \hat{u}_b^+(\omega)\mathrm{e}^{-\mathrm{i}\omega t}, \qquad \theta_b^+(t) = \hat{\theta}_b^+(\omega)\mathrm{e}^{-\mathrm{i}\omega t}, \\ Q_b^+(t) &= \hat{Q}_b^+(\omega)\mathrm{e}^{-\mathrm{i}\omega t}, \qquad M_b^+(t) = \hat{M}_b^+(\omega)\mathrm{e}^{-\mathrm{i}\omega t}, \end{aligned} \tag{20}$$

Likewise, the interface parameters at negative abscissas are assigned the superscript $-$. In this case, the A_3 and A_4 terms are included.

From equations (18) and (19) it follows that the interface reaction forces can be formulated as functions of the displacement and rotation. Hence, the following frequency response relation arises:

$$\begin{bmatrix} \hat{M}_b(\omega) \\ \hat{Q}_b(\omega) \end{bmatrix} = \mathbf{B}(\omega)\begin{bmatrix} \hat{\theta}(\omega) \\ \hat{u}_b(\omega) \end{bmatrix}, \qquad \mathbf{B}(\omega) = \begin{cases} \mathbf{L}_1^+(\mathbf{L}_0^+)^{-1}, & x_b > 0, \\ \mathbf{L}_1^-(\mathbf{L}_0^-)^{-1}, & x_b < 0. \end{cases} \tag{21}$$

The coefficients of the frequency response matrix, $\mathbf{B}(\omega)$, are generally complex. Subsequently, equation (21) is approximated in the following manner:

$$\begin{bmatrix} \hat{M}_b(\omega) \\ \hat{Q}_b(\omega) \end{bmatrix} = \left(\Re(\mathbf{B}) + \frac{\mathrm{i}\omega}{\omega_1}\Im(\mathbf{B})\right)\begin{bmatrix} \hat{\theta}_b(\omega) \\ \hat{u}_b(\omega) \end{bmatrix}, \tag{22}$$

where $\Re(\mathbf{B})$ and $\Im(\mathbf{B})$ represent the real and imaginary parts of $\mathbf{B}(\omega)$ respectively. For harmonic excitation with the circular frequency $\omega = \omega_1$, equation (22) represents a set of completely transparent boundary conditions in the frequency domain, i.e., for a single-frequency signal no reflection occurs. However, when the response is not purely harmonic with a single frequency, some reflection takes place at the interfaces.

Introducing the matrices

$$\mathbf{K}_b = \Re(\mathbf{B}), \qquad \mathbf{C}_b = -\frac{1}{\omega_1}\Im(\mathbf{B}), \tag{23}$$

equation (22) may be formulated as the following transmitting boundary conditions in the time domain:

$$\begin{bmatrix} M_b(t) \\ Q_b(t) \end{bmatrix} = \mathbf{K}_b \begin{bmatrix} \theta_b(t) \\ u_b(t) \end{bmatrix} + \mathbf{C}_b \begin{bmatrix} \dot{\theta}_b(t) \\ \dot{u}_b(t) \end{bmatrix}. \tag{24}$$

Nevertheless, combinations of the material properties and the loading frequency exist where equation (24) will not be physically correct. The problem is that in order to obtain a stable FEM scheme, the system matrices have to be positive definite. This means that the diagonal terms as well as the determinants of the boundary condition matrices must be positive. No problem arises in the imaginary part of **B**, i.e., the damping matrix, but for frequencies above some factor (typically in the range 1.1–2.6) times the cut-off frequency the b_{22} component of **B** relating $Q_b(t)$ to $u_b(t)$ will have negative real part. A solution to the problem is obtained by replacing the first order boundary condition by an equivalent second order boundary condition. Hence, if and only if $k^b_{22} < 0$, equation (24) is modified to

$$\begin{bmatrix} M_b(t) \\ Q_b(t) \end{bmatrix} = \mathbf{K}^*_b \begin{bmatrix} \theta_b(t) \\ u_b(t) \end{bmatrix} + \mathbf{C}_b \begin{bmatrix} \dot{\theta}_b(t) \\ \dot{u}_b(t) \end{bmatrix} + \mathbf{M}^*_b \begin{bmatrix} \ddot{\theta}_b(t) \\ \ddot{u}_b(t) \end{bmatrix}, \tag{25}$$

where

$$\mathbf{K}^*_b = \begin{bmatrix} 2k^b_{11} & 0{\cdot}5k^b_{12} \\ 0{\cdot}5k^b_{21} & -k^b_{22} \end{bmatrix}, \qquad \mathbf{M}^*_b = -\frac{1}{\omega_1^2}\begin{bmatrix} -k^b_{11} & 0{\cdot}5k^b_{12} \\ 0{\cdot}5k^b_{21} & 2k^b_{22} \end{bmatrix}, \tag{26}$$

Analogous to equation (22), equations (24) and (25) will only be exact for harmonic variation at the circular frequency ω_1. When the loading frequency ω diverges from ω_1, the performance of the boundary conditions decreases correspondingly.

One idea of how to overcome the problem with frequency dependence is simply to use a higher order approximation of equation (21) in $i\omega$ corresponding to a transmitting boundary condition of the form

$$\begin{bmatrix} M_b(t) \\ Q_b(t) \end{bmatrix} = \mathbf{G}_0 \begin{bmatrix} \theta_b(t) \\ u_b(t) \end{bmatrix} + \mathbf{G}_1 \begin{bmatrix} \dot{\theta}_i(t) \\ \dot{u}_b(t) \end{bmatrix} + \cdots + \mathbf{G}_n \begin{bmatrix} \theta^{(n)}_b(t) \\ u^{(n)}_b(t) \end{bmatrix}, \tag{27}$$

with $\theta^{(j)}_b$ and $u^{(j)}_b$ denoting the jth derivatives of θ_b and u_b with respect to time. Note that rational filters like equation (27) can still only be valid for ω in a confined interval since it does not provide the correct asymptotic behaviour. Moreover, it has not been possible to calibrate equation (27) to get a stable FE scheme (i.e., a differential filter with all eigenvalues having non-positive real parts) that provides a more accurate solution than that obtained from equations (24) and (25) even within a narrow frequency band.

Wolf [8] proposed a doubly asymptotically correct boundary condition. However, Wolf assumed an asymptotic behaviour proportional to ω for $\omega \to \infty$, which is correct for an elastic medium, but only the b_{12} and b_{21} components of **B** have this asymptotic behaviour, whereas $b_{11} \propto \omega^{1/2}$ and $b_{22} \propto \omega^{3/2}$ in the $\omega \to \infty$ limit. This actually means that a doubly asymptotically correct boundary condition cannot be reduced to an ordinary differential equation. Hence, the approach suggested by Wolf cannot be used in the present problem.

5. FINITE ELEMENT IMPLEMENTATION

As mentioned earlier, the basic idea of the FE approach to the wave propagation problem is that finite elements may be used to describe a complicated local linear or non-linear behaviour of the beam. The transmitting boundary conditions derived in the previous section will be valid as long as the response in the part of the beam *not* modelled by the FEM is linear. This can always be achieved by specifying the boundaries at a sufficient distance from the moving force. However, for simplicity, a linear model also within the FE part of the beam will be considered. Thus, to achieve the weak formulation of the equation of motion, equation (5) is multiplied by an arbitrary weight function, which is chosen as a virtual velocity field, $\tilde{v}$, and integration is carried out by parts,

$$\int_{x_b^-}^{x_b^+} \left[\frac{\partial^2 \tilde{v}}{\partial x^2} EI \frac{\partial^2 u}{\partial x^2} + \tilde{v} \left(\kappa u - \gamma V \frac{\partial u}{\partial x} + \mu V^2 \frac{\partial^2 u}{\partial x^2} \right) \right] \mathrm{d}x + \left[\frac{\partial \tilde{v}}{\partial x} M \right]_{x_b^-}^{x_b^+} + \int_{x_b^-}^{x_b^+} \tilde{v} \left(\gamma \dot{u} - 2\mu V \frac{\partial \dot{u}}{\partial x} + \mu \ddot{u} \right) \mathrm{d}x - [\tilde{v} Q]_{x_b^-}^{x_b^+} = \int_{x_b^-}^{x_b^+} \tilde{v} f(x, t) \, \mathrm{d}x. \tag{28}$$

The Q and M terms in equation (28) are the moment and shear force at the ends of the FE model, which must agree with equation (24) or (25).

Next, the displacement field as well as the virtual velocity field is put in discrete form,

$$u(x, t) = \mathbf{N}(x)\mathbf{a}(t), \qquad \tilde{v}(x, t) = \tilde{\mathbf{N}}(x)\tilde{\mathbf{a}}(t), \tag{29}$$

where $\mathbf{N}(x)$ and $\tilde{\mathbf{N}}(x)$ are global shape functions of the dimension $1 \times 2n$ with n being the number of nodal points. $\mathbf{a}$ and $\tilde{\mathbf{a}}$ represent the nodal displacements and rotations in the physical field and vertical and angular velocities in the virtual field respectively.

Equation (29) is inserted into equation (28). The stationarity condition of the variation principle then leads to the FEM-formulation

$$\mathbf{M}\ddot{\mathbf{a}} + \mathbf{C}\dot{\mathbf{a}} + \mathbf{K}\mathbf{a} = \mathbf{f} + \mathbf{f}_b, \tag{30}$$

where the system matrices and load vectors are defined as

$$\mathbf{M} = \int_{x_b^-}^{x_b^+} \tilde{\mathbf{N}} \mu \mathbf{N} \, \mathrm{d}x, \qquad \mathbf{C} = \int_{x_b^-}^{x_b^+} \tilde{\mathbf{N}} \left(\gamma \mathbf{N} - 2\mu V \frac{\partial \mathbf{N}}{\partial x} \right) \mathrm{d}x, \tag{31}$$

$$\mathbf{K} = \int_{x_b^-}^{x_b^+} \left[\frac{\partial^2 \tilde{\mathbf{N}}}{\partial x^2} EI \frac{\partial^2 \mathbf{N}}{\partial x^2} + \tilde{\mathbf{N}} \left(\kappa \mathbf{N} - \gamma V \frac{\partial \mathbf{N}}{\partial x} + \mu V^2 \frac{\partial^2 \mathbf{N}}{\partial x^2} \right) \right] \mathrm{d}x, \tag{32}$$

$$\mathbf{f} = \int_{x_b^-}^{x_b^+} \tilde{\mathbf{N}} f \, \mathrm{d}x, \qquad \mathbf{f}_b = [\hat{\mathbf{N}} Q]_{x_b^-}^{x_b^+} - \left[\frac{\partial \tilde{\mathbf{N}}}{\partial x} M \right]_{x_b^-}^{x_b^+}. \tag{33}$$

The global boundary conditions, equation (24) or (25), must be applied via the boundary load vector $\mathbf{f}_b$ at the corresponding end nodes of the two outmost elements. Actually, this corresponds to an adjustment in the system matrices $\mathbf{M}$, $\mathbf{C}$ and $\mathbf{K}$ rather than the load vector $\mathbf{f}$.

When linear elements are used in the FEM discretization of wave propagation with convection, e.g., in the elastic half-space, it is a well-known fact that standard Galerkin variation with $\tilde{\mathbf{N}}(x) = \mathbf{N}(x)$ causes instability due to negative numerical damping

proportional to the convection velocity. This may be counteracted using Petrov–Galerkin variation, where a skew-symmetric term is applied to $\tilde{\mathbf{N}}(x)$ [14]. Alternatively, the novel approach suggested by Krenk *et al.* [11] may be taken. Here the standard Galerkin approach is used, but in the discretized field equations an appropriate amount of additional damping is introduced to counterbalance the negative numerical damping. The same instability problems are encountered in the present case when the convection velocity becomes sufficiently high. However, when Ω is of magnitude 1, no problems arise using the direct Galerkin method for values of v less than approximately 2. Henceforth, the standard cubic Hermite shape functions for Euler beam elements can be used in the numerical analysis at convection velocities fulfilling this requirement.

6. NUMERICAL EXAMPLES

A finite beam section of the length L is modelled, and numerical integration is performed over the time interval T_I. In this procedure, both the time increment, Δt, and the spatial increment, Δx have to be considered. The latter corresponds to the element length in the FEM model.

As a rule of thumb, when linear elements are used each wave must be described by at least $n_e^\lambda = 10$ elements to obtain satisfactory results [15]. For Euler beam elements the number is somewhat lower, about 4, because the Hermite shape functions are cubic. Note that because a moving system of reference is used, it is always possible to apply a point load directly in one of the nodes. Hence, this number of elements can be used, not only for analysis of stationary loads but also for moving loads, unlike the case when a fixed system of reference is used [7]. In any case, it is necessary to know the shortest wavelength present at either side of the loading. The wavelengths are given as

$$\lambda_{min}^{+} = \min\left\{\frac{2\pi}{|\alpha_1|}, \frac{2\pi}{|\alpha_2|}\right\}, \quad \lambda_{min}^{-} = \min\left\{\frac{2\pi}{|\alpha_3|}, \frac{2\pi}{|\alpha_4|}\right\}. \tag{34}$$

Next, the length of each element is found as

$$\Delta x^{+} = \frac{\lambda_{min}^{+}}{n_e^\lambda}, \qquad \Delta x^{-} = \frac{\lambda_{min}^{-}}{n_e^\lambda}. \tag{35}$$

The time step is obtained from the Courant relation

$$\frac{|c|\,\Delta t}{\Delta x} = C, \qquad C \leqslant 1, \tag{36}$$

where c and Δx present a characteristic set of wave propagation velocity and spatial increment and C is the Courant number.

To ensure that equation (36) is fulfilled for all possible sets $(c, \Delta x)$ it is necessary that

$$\Delta t = \min\left\{\frac{C\Delta x^{+}}{|c_1|}, \frac{C\Delta x^{+}}{|c_2|}, \frac{C\Delta x^{-}}{|c_3|}, \frac{C\Delta x^{-}}{|c_4|}\right\}. \tag{37}$$

When the convection velocity is chosen to be sufficiently high or a certain amount of damping is introduced, the increments defined by equations (35) and (37) provide no

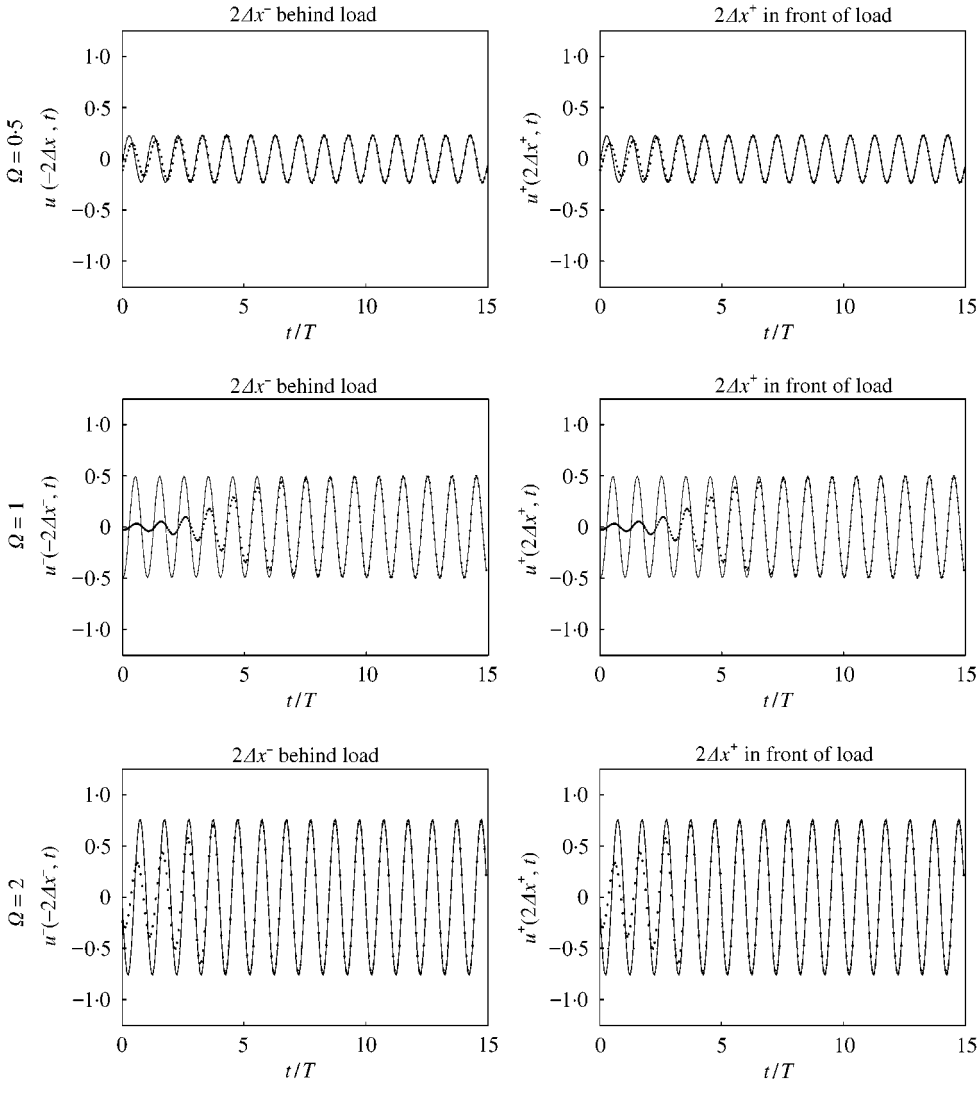

Figure 6. Numerical (· · · ·) versus analytical (——) results, $v = 0$.

difficulties in the numerical integration. However, when $\Omega = 1$ the real part of one of the wavenumbers will be extremely small, no matter how much damping and convection that has been introduced (see Figures 3–5). Hence, equation (37) prescribes a time step only slightly larger than zero, i.e., $\Delta t \approx 0$, and consequently a huge amount of integration steps must be performed within the time interval T_I. It should be noted that when $\zeta = v = 0$, no numerical solution can be formed for $\Omega = 1$ since all $\alpha_j = 0$ in this particular case. Here, however, as stated earlier the amplitude of motion is infinite.

Figures 6 and 7 show the results for a model with the parameters

$$EI = 10^8 \text{ N m}^2, \qquad \kappa = 10^8 \text{ N/m}^2, \quad \mu = 10^2 \text{ kg/m}, \quad \zeta = 0{\cdot}1, \tag{38}$$

$$n_e^\lambda = 8, \qquad C = 0{\cdot}5, \qquad L = \frac{\lambda^- + \lambda^-}{2}. \tag{39}$$

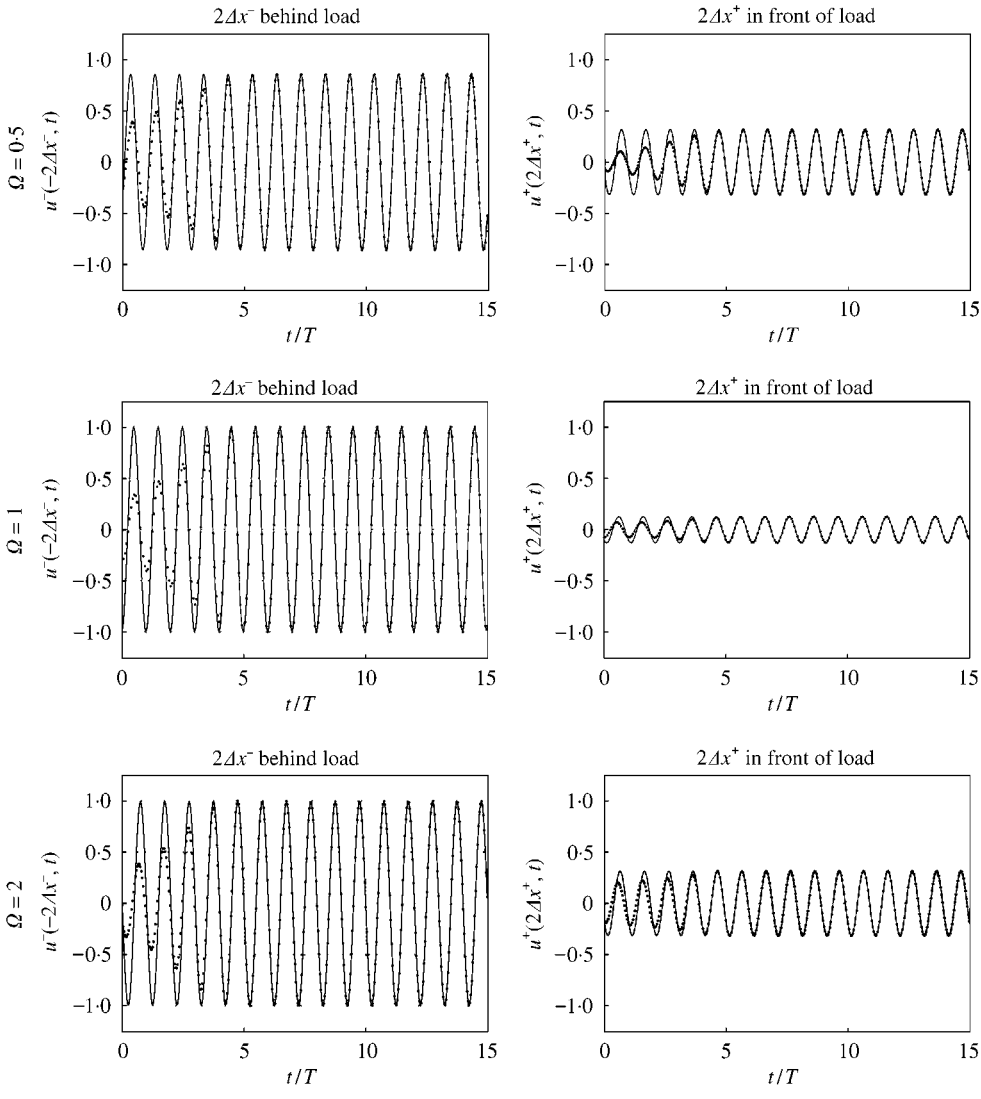

Figure 7. Numerical (· · · ·) versus analytical (——) results, $v = 1$.

The analysis is performed for single-frequency harmonic excitation at various combinations of loading frequency and convection velocity,

$$\Omega = \{0{\cdot}5, 1, 2{\cdot}0\}, \qquad v = \{0, 1\}, \tag{40}$$

and the displacement time series are displayed for two nodes, which are located two element lengths to either side of the point load. The numerical results (*the dotted line*) are plotted against the corresponding analytical solution (*the continuous line*). Note that the analytical solutions are stationary, whereas the numerical solutions include a transient part which arises because the load also excites the eigenmodes of the FEM-model, which are not present in the analytical solution directly concerning the infinite beam. The transient motion has been counteracted by Rayleigh damping that is fully removed after 10 excitation periods, $T = 2\pi/\omega$.

In all cases, the numerical results after $t/T = 10$ are seen to be nearly identical to the analytical results. Hence, the transmitting boundary conditions are seen to work well. Note that the problem previously described with the time step given by equation (37) arises for the combination ($v = 1$, $\Omega = 1$) (see Figure 4). This problem has been overcome by disregarding the problematic wave velocity close to infinity in the choice of time step. Nonetheless, the results of the numerical and the analytical solution are in good agreement also in these cases, in defiance of the fact that one of the waves cannot propagate in the numerical model because $C \gg 1$. This is of particular interest, since the amplitude of the wave component in question is actually relatively high and the attenuation is low, see Figure 4.

Next, the numerical solution is tested when the excitation signal contains several frequencies. The load is applied as a Ricker pulse, which is defined as

$$f(t) = \begin{cases} f_0 \dfrac{5^{2\cdot5}}{4^2} v(1 - v^2)^2 & \text{for } 0 < t < T_c, \\ 0 & \text{for } T_c \leqslant t, \end{cases} \tag{41}$$

where f_0 is the maximum intensity of the load signal and v is a linear function given as

$$v(t) = \frac{2t}{T_c} - 1. \tag{42}$$

The amplitude spectrum of the Ricker pulse has a distinct peak at the circular frequency $\omega_c = 2\pi/T_c$ (see Figure 8). Hence ω_c is referred to as the *centre frequency*.

When the loading is not harmonic, the question arises as to which frequency the transmitting boundary conditions should be tuned to. A natural choice when concerning the Ricker pulse is to use $\omega_1 = \omega_c$ as the tuning frequency because the majority of the energy of the loading is contained in a signal with this frequency. However, in contrast to the case when stationary loading is applied, the structure will not undergo stationary forced vibrations at the loading frequency. After the travelling wave has passed, the beam will instead continue vibrating at the eigenfrequency, ω_0. This actually means that it might be more accurate to tune the transmitting boundary conditions to a frequency somewhere between ω_c and ω_0 according to the following linear weighting:

$$\omega_1 = W_c \omega_c + (1 - W_c)\, \omega_0, \quad 0 \leqslant W_c \leqslant 1. \tag{43}$$

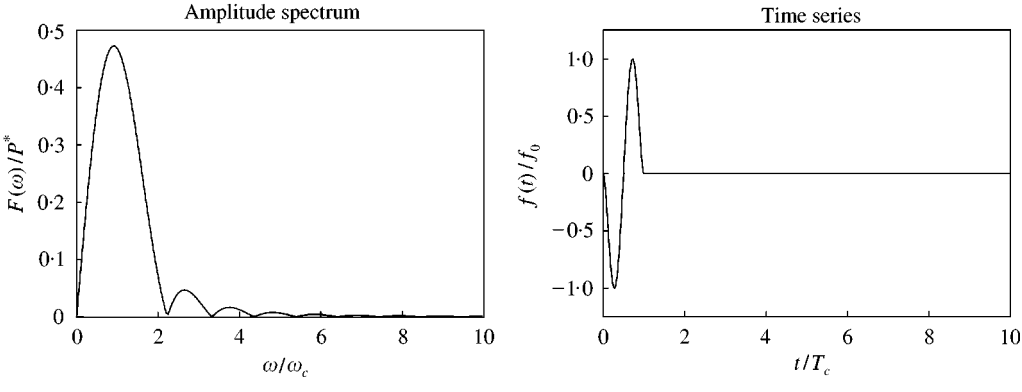

Figure 8. Ricker pulse, amplitude spectrum and time series; $P^* = f_0 T_c$.

Another problem is that no analytical solution to the wave propagation problem can be found. Instead the time-integration solution is checked against a solution obtained using a discrete Fourier transform–inverse discrete Fourier transform (DFT–IDFT) method. As a first step in this method time and frequency are discretized,

$$t_j = (j-1)\Delta t, \qquad j = 1, 2, \ldots, J, \qquad \Delta t = \frac{T_I}{J-1},$$
$$\omega_k = (k-1)\Delta\omega, \qquad k = 1, 2, \ldots, J, \qquad \Delta\omega = \frac{2\pi}{\Delta t}, \tag{44}$$

where T_I is the total analysis time and J is most favourably chosen as a power of two so that the fast Fourier transform (FFT) algorithm can be used. The nodal displacement amplitudes are then calculated for each ω_k as

$$\mathbf{A}(\omega_k) = \mathbf{H}(\omega_k)\mathbf{F}(\omega_k), \tag{45}$$

where $\mathbf{A}$ and $\mathbf{F}$ are the DFTs of $\mathbf{a}$ and $\mathbf{f}$ defined as

$$\mathbf{A}(\omega_k) = \sum_{j=1}^{J} \mathbf{a}(t_j)\exp(\mathrm{i}\omega_k t_j)\Delta t, \qquad \mathbf{F}(\omega_k) = \sum_{j=1}^{J} \mathbf{f}(t_j)\exp(\mathrm{i}\omega_k t_j)\Delta t, \tag{46}$$

and $\mathbf{H}$ is the frequency response matrix,

$$\mathbf{H}(\omega_k) = (\mathbf{K}(\omega_k) - \mathrm{i}\omega_k\mathbf{C}(\omega_k) - \omega_k^2\mathbf{M}(\omega_k))^{-1}. \tag{47}$$

Note that the system matrices depend on the frequency because the transmitting boundary conditions are applied via $\mathbf{M}$, $\mathbf{C}$ and $\mathbf{K}$.

Subsequently, the nodal displacements and rotations can be found by taking the IDFT of $\mathbf{A}$, i.e.,

$$\mathbf{a}(t_j) = \frac{1}{2\pi}\sum_{k=1}^{J} \mathbf{A}(\omega_k)\exp(-\mathrm{i}\omega_k t_j)\Delta\omega. \tag{48}$$

If the beam is at rest, both at the beginning and at the end of the analysis time interval T_I, the solution is correct except for the error introduced via the transmitting boundary conditions for each single frequency ω_k. However, the previous analysis of the performance of the transmitting boundary conditions at single-frequency harmonic excitation proves that this error is insignificant. Also note that the DFT–IDFT method does not suffer from any instability problems (since no time integration is performed). Thus, it can be used in conjunction with standard Galerkin variation for arbitrary convection velocity and loading frequency.

Figure 9 shows the displacement time series for the nodes two element lengths behind and in front of the loading respectively. The results from a direct time integration of the FEM scheme with and without transmitting boundary conditions are plotted against the "exact" solution obtained by the DFT–IDFT method. The centre frequency of the Ricker pulse is $\omega_c = 2\omega_0$ and the relative convection is $v = 0{\cdot}5$. Different values of ω_1 are tested and the following observations can be made.

In all cases the introduction of boundary conditions proves favourable. Thus, the numerical solution *without* transmitting boundaries is far off, whereas the numerical solution *with* transmitting boundary conditions is close to the exact solution.

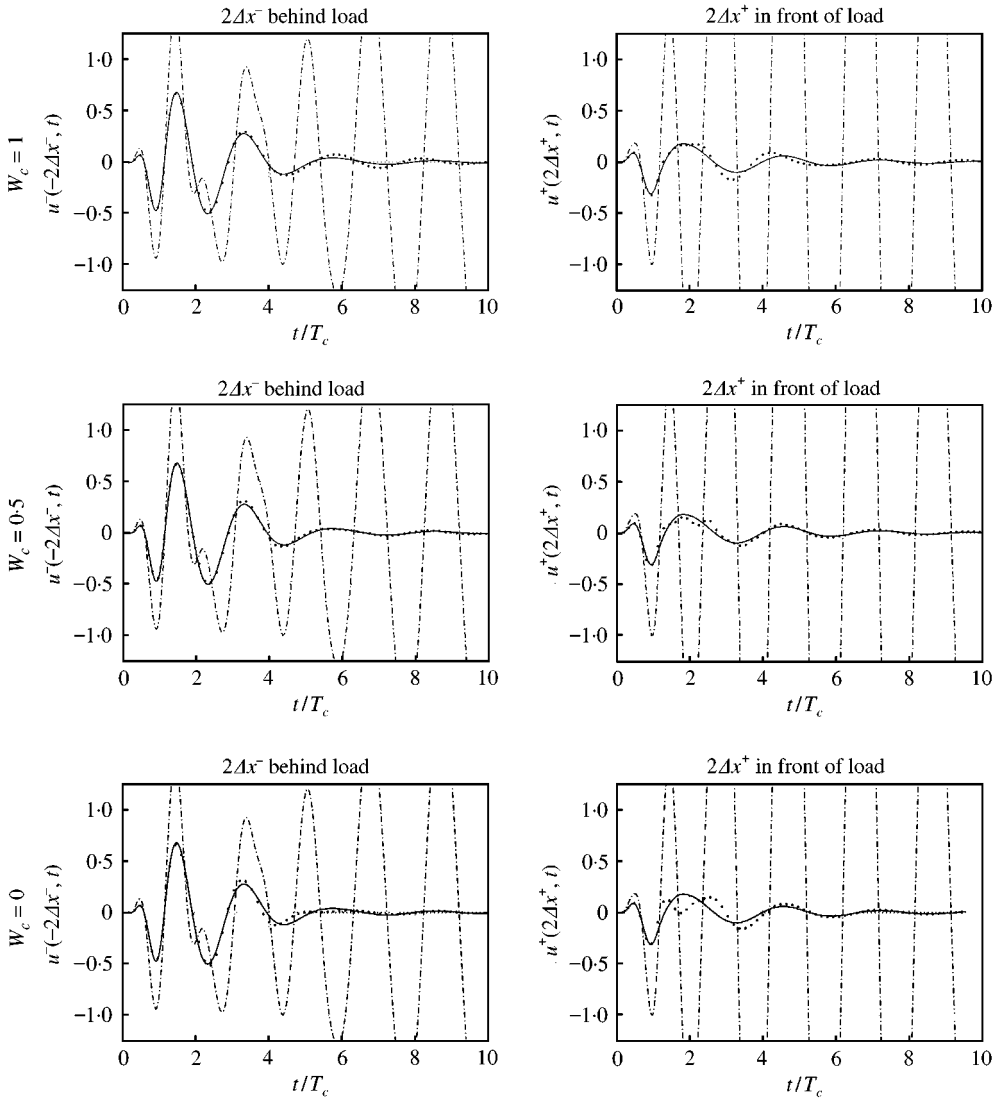

Figure 9. Numerical results with (· · ·) and without (—·—·) transmitting boundary conditions versus "exact" results (–) for $\Omega_c = 2{\cdot}0$ and $\nu = 0{\cdot}5$.

Moreover, the solution for $W_c = 0{\cdot}5$ is only slightly less accurate than the solution for $W_c = 1$ in the first part of the integration time, i.e., before the travelling wave generated by the pulse leaves the modelled part of the beam. However, it is much more accurate in the remaining part of the T_I interval. Likewise, it is superior to the solution with $W_c = 0$ in the first few periods T_c and suffers only little in the remainder of the integration time. Hence, all in all a tuning with $W_c = 0{\cdot}5$ turns out to be better than tuning the boundary conditions to either ω_c or ω_0.

7. CONCLUSIONS

When a harmonic, vertical point load moves uniformly along an Euler beam resting on a Kelvin foundation, four independent waves occur, two on either side of the moving source.

The nature of the waves is highly dependent on the different parameters in the problem but in most cases two of the waves will be travelling waves with almost no attenuation, and the remaining two waves will be near-field waves trapped within a region close to the source. It turns out that one of the wave components may have an extremely high phase velocity, which is a problem in the numerical solution. However, even if this wave component has a significant amplitude at the artificial boundary it may be disregarded when determining the time step for the numerical integration.

Transmitting boundary conditions can be formulated for harmonic excitation with a single-frequency signal. The transmitting boundary conditions are tested in an FEM-model and are found to work satisfactorily for single-frequency harmonic excitation. For a Ricker pulse containing a band of frequencies the transmitting boundary conditions also work quite well. It becomes advantageous to tune the boundary conditions to a frequency somewhere between the centre frequency of the loading and the eigenfrequency of the system.

Because the relationship between time and spatial derivatives of the displacement field is strongly non-linear in the beam problem it seems impossible to devise a filter, which is independent of the loading frequency, even within a narrow frequency band. Nevertheless, quite good results can be obtained, even for a broad-banded load, when the single-frequency transmitting boundary conditions are tuned to a suitable frequency.

ACKNOWLEDGMENTS

The present research was supported by The Danish Technical Research Council within the project: 'Damping Mechanisms in Dynamics of Structures and Materials'.

REFERENCES

1. X. SHENG, C. J. C. JONES and M. PETYT 1999 *Journal of Sound and Vibration* **228**, 129–156. Ground vibration generated by a load moving along a railway track.
2. H. A. DIETERMAN and A. METRIKINE 1997 *ASME Journal of Applied Mechanics* **64**, 596–600. Critical velocities of a harmonic load moving uniformly along an elastic layer.
3. A. METRIKINE and H. A. DIETERMAN 1997 *ASME Journal of Applied Mechanics* **64**, 951–956. Three-dimensional vibrations of a beam on an elastic half-space: resonance interaction of vertical-longitudinal and later beam waves.
4. H. A. DIETERMAN and A. METRIKINE 1997 *European Journal of Mechanics, A/Solids* **16**, 295–306. Steady-state displacements of a beam on an elastic half-space due to a uniformly moving constant load.
5. S. LU and D. XUEJUN 1998 *Journal of Applied Mathematics and Mechanics* **19**, 367–373. Dynamic analysis to infinite beam under a moving line load with uniform velocity.
6. M. S. A. HARDY 1995 *Journal of Sound and Vibration* **180**, 637–644. The generation of waves in infinite structures by moving harmonic loads.
7. J. R. RIEKKER, Y.-H. LIN and M. W. TRETHEWEY 1996 *Finite Elements in Analysis and Design* **21**, 129–144. Discretization considerations in moving load finite element beam models.
8. J. P. WOLF 1991 *Earthquake Engineering and Structural Dynamics* **20**, 11–32. Consistent lumped-parameter models for unbounded soil: physical representation.
9. J. P. WOLF and C. SONG 1996 *Finite-Element Modelling of Unbounded Media*. Chichester: Wiley & Sons Ltd.
10. A. PARONESSO and J. P. WOLF 1998 *Earthquake Engineering and Structural Dynamics* **27**, 609–618. Recursive evaluation of interaction forces and property matrices from unit-impulse response functions of unbounded medium based on balancing approximation.
11. S. KRENK, L. KELLEZI, S. R. K. NIELSEN and P. H. KIRKEGAARD 1999 *Proceedings of the 4th European Conference on Structural Dynamics, Eurodyn '99, Praha, June* 7–1, Vol. 1, 447–452. Finite elements and transmitting boundary conditions for moving loads.

12. A. METRIKINE and H. A. DIETERMAN 1997 *Journal of Sound and Vibration* **201**, 567–576. Instability of vibrations of a mass moving uniformly along an axially compressed beam on a viscoelastic foundation.
13. A. S. J. SUIKER, R. DE BORST and C. ESVELD 1998 *Archives of Applied Mechanics* **68**, 158–168. Critical behaviour of a Timoshenko beam-half plane system under a moving load.
14. O. C. ZIENKIEWICZ and R. L. TAYLOR 1991 *The Finite Element Methods*, Vol. 2. London: McGraw-Hill; fourth edition.
15. I. HARARI, K. GROSH, T. J. R. HUGHES, M. MALHOTRA, P. PINSKY, J. R. STEWART and L. L. THOMPSON 1996 *Archives of Computational Methods in Engineering* **3**, 131–309. Recent developments in finite element methods for structural acoustics.